Astron. Astrophys. 139, 181–195 (1984)

ASTRONOMY AND ASTROPHYSICS

# CO ($J=2\rightarrow1$) observations of molecular clouds associated with H II regions from the southern hemisphere*

**J. Brand[1], M. D. P. van der Bij[1], C. P. de Vries[1], F. P. Israel[2], T. de Graauw[2], H. van de Stadt[3], J. G. A. Wouterloot[4], A. Leene[1], and H. J. Habing[1]**

[1] Sterrewacht, P.O. Box 9513, 2300 RA Leiden, The Netherlands
[2] Astronomy Division, Space Science Dept., ESTEC, Noordwijk, The Netherlands
[3] Astronomical Institute, Servaas Bolwerk 13, Utrecht, The Netherlands
[4] ESO, Karl-Schwarzschild-Strasse 2, D-8046 Garching bei München, Federal Republic of Germany

Received March 16, accepted June 8, 1984

**Summary.** We have searched for CO($J=2\rightarrow1$) emission at 47 positions in the direction of southern H II regions, mainly taken from the RCW-catalogue. Nineteen positions yielded negative results [i.e. $T_A^*(2\rightarrow1)<1$ K]. The observations are compared with CO results obtained by other workers and briefly discussed. There seems to be no significant difference between the $T_A^*(J=2\rightarrow1)$ and $T_A^*(J=1\rightarrow0)$ transitions. In general no systematic velocity difference between the molecular and ionized gas is found. Three objects were observed in more detail: G265.1+1.5 (RCW 36), G327.3−0.6, and G35.2−1.8 (W 48). The source G327.3−0.6, associated with RCW 97, is a relatively small CO cloud, showing the characteristics of bipolar outflow. The CO emission associated with W 48 is complex; there is evidence for self absorption. In the direction of RCW 36 there are at least two clouds or cloud components along the line of sight.

**Key words:** molecular clouds – CO($J=2\rightarrow1$) emission – southern H II regions

## 1. Introduction

In the northern hemisphere, the close relationship between H II regions and molecular clouds traced by CO emission has been well established (Blair et al., 1975; Blitz et al., 1982).

A first survey of CO($J=1\rightarrow0$) emission expected to be associated with southern hemisphere H II regions was carried out by Gillespie et al. (1977). Since that time, more survey-type observations have become available, both in the CO($J=1\rightarrow0$) transition (Whiteoak et al., 1982) and the CO($J=2\rightarrow1$) transition (Martin et al., 1983). Several individual southern H II region complexes have been observed in detail (e.g. De Graauw et al., 1980; Gillespie et al., 1977).

In this paper we describe CO($J=2\rightarrow1$) observations of molecular clouds associated with H II regions situated in the third and fourth quadrant of our Galaxy. These observations are part of an extensive program which had the objective to systematically survey the plane of the Galaxy ($b=0°$) between $l=270°$ and $l=357°$, and to observe dark clouds, reflection nebulae, HH-type objects and H II regions. The results of the plane survey and the observations of the dark clouds, reflection nebulae and HH-type objects are published separately (De Vries et al., 1984; Israel et al., 1984). Preliminary reports were given by De Graauw, Israel, and De Vries (1983), and Brand (1983). The main purpose of the present H II region survey is to increase the sample of southern H II regions with known CO emission (or the lack of it) and to provide a framework for further, more detailed observations. In addition to the survey data, we obtained more detailed information on a small number of sources, notably G265.1+1.5 (RCW 36), G327.3−0.6 (associated with RCW 97) and G35.2−1.8 (W 48). In the following, we will first describe the observations, briefly review the survey results, and in somewhat more detail discuss the mapping results.

## 2. Observations

The observations described in this paper were made with three different telescopes. The main survey was carried out in 1981 and 1982 with the ESO 1.4 m Coudé Auxiliary Telescope (CAT) at La Silla, Chile. Mapping was done with the 2.5 m DuPont telescope at Las Campanas Observatory[1], Chile (1981), the ESO 3.6 m telescope at La Silla, Chile (1980), and the CAT (1981, 1982). Relevant information on telescopes and observations is summarized in Table 1. A brief description follows below.

During the observations with the 2.5 m and the 3.6 m telescopes the receiver was mounted at the Cassegrain focus and matched to the telescopes via a polyethylene lens. At the CAT, with a three mirror Coudé focus, a different set-up had to be used. The receiver was installed next to the telescope and the radiation was reflected into the receiver by means of a flat mirror on top of an aluminum tube. Matching was done by mounting an $f/29$ secondary mirror in the telescope and a polyethylene lens, placed inside the aluminum tube. This combination resulted in an $f/10$ focal ratio which matched that of the receiver.

The pointing of the telescopes was regularly checked on the position of field stars. The pointing accuracy of the CAT was

*Send offprint requests to:* J. Brand

* Most of the observations were collected at the European Southern Observatory at La Silla, Chile

1 Las Campanas Observatory is operated by the Carnegie Institution of Washington

**Table 1.** Characteristics of the telescopes and the receiver system

| | Las Campanas | ESO La Silla | ESO La Silla |
|---|---|---|---|
| Telescope | 2.5 m DuPont | 3.6 m | 1.4 m CAT |
| Altitude | 2400 m | 2450 m | 2450 m |
| Observing periods | April/May 1980 | May 1980 | June to October 1981<br>April to July 1982 |
| HPBW | 2'.3 | 1'.9 | 5'.5 |
| Telescope efficiency | 0.45 | 0.55 | 0.35 |
| $T_{sys}$(DSB) | 2200 K | 2200 K (1980) | 1750 K (1981)<br>1400 K (1982) |
| Beam efficiency | 0.60 | 0.60 | 0.43 |
| Calibrators | | | |
| $T_A^*$ (Orion-A) | – | 64 K | 36 K |
| $T_A^*$ (M17(SW)) | – | – | 16 K |
| Observations | G327.3−0.6 | G35.2+1.8 | HII region survey<br>G 265.1+1.5 |

usually only within 1′ to 2′. The pointing accuracy of the other telescopes was good.

We used a heterodyne receiver, developed and built at the European Space Research and Technology Centre (ESTEC) at Noordwijk, The Netherlands, in collaboration with the observatory at Utrecht. This system uses a backward wave oscillator (carcinotron) as a local oscillator (LO) and Schottky barrier diode mixers at ambient temperature. This resulted in (DSB) system temperatures varying from $T_{DSB}=2200$ K to $T_{DSB}=1400$ K (see Table 1).

The incoming signal was fed into two 256-channel filterbanks, with a width per channel of 1 MHz and 250 kHz, respectively, corresponding to a velocity resolution of 1.3 km s$^{-1}$ and 0.33 km s$^{-1}$ at the observing frequency of 230 GHz. Consequently, the available velocity intervals were, respectively, 333 km s$^{-1}$ and 83 km s$^{-1}$ (both centered at the same velocity). A more detailed description of the receiver and the backend is given by Lidholm and De Graauw (1979).

From skydips we determined the zenith opacity and an overall efficiency that includes losses in the telescope and backward spillover. This has been termed telescope efficiency by Ulich and Haas (1976). A discussion on the atmospheric transmission from June to October 1981 at La Silla has been presented elsewhere (Brand, 1982). Spectra were taken in the position switching mode. All temperatures given here are corrected antenna temperatures $T_A^*$ (Kutner and Ulich, 1981).

A particular problem was the presence of baseline ripple in the spectra due to LO power and mixer noise leaking into the telescope and being reflected back into the receiver. This problem was largely solved by applying absorbing material at the secondary mirror. At the CAT, due to its construction, it was also necessary to use a vibrating mirror inside the receiver.

### 3. HII region survey

In 1981 and 1982 the ESO 1.4 m CAT at La Silla was used to observe a number of HII regions by means of single-point observations of the CO($J=2\rightarrow1$) transition. The objects were selected from the catalogue of H$\alpha$ emission regions compiled by Rodgers et al. (1960; hereafter RCW) and from Gillespie et al. (1977; hereafter G77). The latter took their CO-positions from 5 GHz continuum-, H109$\alpha$-, and $H_2CO$-surveys. In Table 2a the observational results are summarized. Some representative spectra are shown in Fig. 1.

The data in Table 2a are mostly derived from the high resolution ($\Delta v=250$ kHz) spectra. Column 1 gives the source number in galactic coordinates (Goss and Shaver, 1970), column 2 lists other names for the source, columns 3 and 4 the equatorial coordinates of the observed position, column 5 the velocity of the peak of the line profile, with respect to the local standard of rest (LSR), and column 7 gives the equivalent width $\Delta V\left[=\int_{\text{line}} T_A^* dV/T_A^*(\text{peak})\right]$. Column 8 is reserved for remarks. We used Orion-A and M17(SW) as our prime calibrators, with $T_A^*=35.6$ K for Orion-A and $T_A^*=15.8$ K for M17(SW); these sources were observed a few times every day. From the scatter in the $T_A^*$-values of these calibrators, we derive an uncertainty of 15% to 20% for an individual $T_A^*$-value in Table 2a. Since many of the line profiles are quite broad, the quoted $V_{LSR}$-values can have an uncertainty larger than the velocity resolution of the spectra (0.33 km s$^{-1}$). Of the 47 positions observed, 19 went undetected. Of the latter, eighteen were not included in previous CO surveys (G77; Whiteoak et al., 1982; hereafter WOR 82; Martin et al., 1983; hereafter M83). At least some of the non-detections will be caused by a displacement of the molecular cloud from the center of the HII region, as we pointed in many cases to the latter and not to nearby obscuration (i.e. in all those instances where the position was taken from the RCW-catalogue, which discriminates against extinction). Of the 28 detected regions, 18 were observed in the other above-mentioned CO surveys. These have been listed in Table 2b.

Because the data in Table 2b were collected with different beam sizes and different velocity resolutions, one should be cautious in comparing them. For instance, for a sharply intensity-peaked

**Table 2a.** CAT survey of galactic HII-regions; results

| Source designation | | Observed position (1950) | | CO($J=2\rightarrow1$) data | | | Remarks |
|---|---|---|---|---|---|---|---|
| G | Other | h m s | ° ′ ″ | $T_A^*$ (K) | $V_{LSR}$ (km s$^{-1}$) | $\Delta V$ (km s$^{-1}$) | |
| 208.9−19.4 | Orion-A | 05 32 47 | −05 24 21 | 35.6 | + 8.7 | | |
| 223.9−1.9 | RCW 2 | 07 02 00 | −10 27 | 5.4 | +17.5 | 2.6 | |
| 224.2+1.2 | RCW 3 | 07 14 00 | −09 18 | < 1 | | | |
| 227.8−0.2 | RCW 5 | 07 16 06 | −13 09 | < 1 | | | |
| 231.6−4.3 | RCW 6 | 07 08 00 | −18.24 | < 1 | | | |
| 232.6+0.9 | RCW 7 | 07 29 30 | −16 51 | < 1 | | | |
| 233.9−0.1 | RCW 8 | 07 28 18 | −18 27 | 2.3 | +43.2 | 2.8 | |
| 234.4−0.2 | RCW 10 | 07 29 00 | −18 54 | < 1 | | | |
| 234.7+0.9 | RCW 12 | 07 33 42 | −18 42 | < 1 | | | |
| 234.8−0.1 | RCW 13 | 07 30 06 | −19 18 | < 1.5 | | | |
| 235.6−4.1 | RCW 14 | 07 17 00 | −21 50 | < 1.5 | | | |
| 243.3+0.6 | RCW 16 | 07 51 12 | −26 15 | < 1 | | | |
| 243.5−1.0 | RCW 17 | 07 45 24 | −27 13 | < 1 | | | |
| 253.8−0.5 | RCW 19 | 08 18 30 | −35 42 | < 1 | | | |
| | 19B | 08 14 30 | −35 27 | < 1 | | | |
| 254.5+0.0 | RCW 20 | 08 17 30 | −36 00 | < 1 | | | |
| 259.2+1.3 | RCW 25 | 08 36 54 | −39 02 | < 1 | | | |
| 261.6+0.9 | RCW 32 | 08 43 00 | −41 09 | 1.7 | + 6.3 | 2.2 | |
| 263.0+1.4 | RCW 33 | | | 5.4 | + 6.7 | 2.6 | Average from three spectra at three different positions (positions 2–4 in Fig. 8) |
| 264.4+1.4 | RCW 34 | 08 54 40 | −42 55 00 | 2.0 | + 6.3 | 3.3 | |
| 264.6+0.1 | RCW 35 | 08 49 42 | −43 55 | < 1 | | | |
| 265.1+1.5 | RCW 36 | 08 57 38 | −43 33 24 | 5.5, 9.4 | + 5.4, +7.9 | 2.9, 2.5 | |
| 267.0+0.1 | RCW 37 | 08 58 30 | −45 45 | 2.5 | + 5.1 | 2.5 | |
| 267.9−1.1 | RCW 38 | 08 57 25 | −47 19 18 | 9.1, 5.2 | − 0.9, +5.2 | 3.6, 3.8 | |
| 269.2−1.1 | RCW 39 | 09 01 54 | −48 12 | < 1 | | | |
| 269.3−1.4 | RCW 40 | 09 01 00 | −48 27 | 4.4 | + 6.1 | 3.4 | |
| 274.0−1.1 | RCW 42 | 09 22 47 | −51 47 00 | 2.8 | +40.8 | 5.8 | |
| 283.0−2.7 | RCW 47 | 10 03 30 | −58 42 | < 1 | | | |
| 283.5−1.0 | RCW 48 | 10 14 00 | −57 36 | < 1 | | | |
| 284.3−0.3 | RCW 49 | 10 22 | −57 27 | < 1 | | | |
| 291.3−0.7 | RCW 57 | 11 09 47 | −61 02 36 | 9.9 | −21.1 | 10.1 | |
| 305.3+0.2 | RCW 74B | 13 08 23 | −62 17 36 | 8.5 | −37.4 | 7.5 | Poor quality spectrum |
| 305.4+0.2 | RCW 74C | 13 09 21 | −62 18 54 | 7.6, 6.8 | −40.0, −35.5 | 7.3 | |
| 306.3+0.2 | RCW 75 | 13 16 30 | −62 15 00 | 6.4 | −28.4 | 4.0 | |
| 322.2+0.6 | RCW 92 | 15 14 50 | −56 28 00 | 7.7 | −55.6 | 5.8 | |
| 327.3−0.6 | | 15 49 13 | −54 26 30 | 12.2 | −47.1 | 8.4 | |
| 332.8−0.6 | RCW 106 | 16 16 25 | −50 47 30 | 5.2 | −56.3 | 8.2 | |
| 333.0−0.4 | | 16 16 52 | −50 33 00 | 9.5 | −54.0 | 10.3 | |
| 336.5−1.5 | RCW 108 | 16 36 20 | −48 45 36 | 12.7 | −23.4 | 4.9 | |
| 348.7−1.0 | RCW 122 | 17 16 40 | −38 54 06 | 16.6 | −12.3 | 6.9 | |
| 351.4+0.7 | RCW 127D | 17 17 18 | −35 46 54 | 9.2 | − 5.0 | 7.7 | Poor quality spectrum |
| 351.4+0.7 | RCW 127E | 17 17 35 | −35 43 42 | 20.8 | − 5.9 | 11.0 | |
| 351.6−1.3 | | 17 25 56 | −36 37 54 | 13.7 | − 9.7 | 7.7 | |
| 353.1+0.6 | W 22 | 17 22 18 | −34 19 54 | 7.8 | − 4.5 | 10.2 | |
| 353.2+0.9 | W 22B | 17 21 30 | −34 08 06 | 5 | − 3 | 13 | Poor quality spectrum |
| 15.0−0.7 | M 17 (SW) | 18 17 26.5 | −16 14 54 | 15.8 | +18.7 | 7.8 | |
| 49.5−0.4 | W 51 | 19 21 27 | +14 24 30 | 10.8 | +44.0 | 11.6 | Poor quality spectrum |

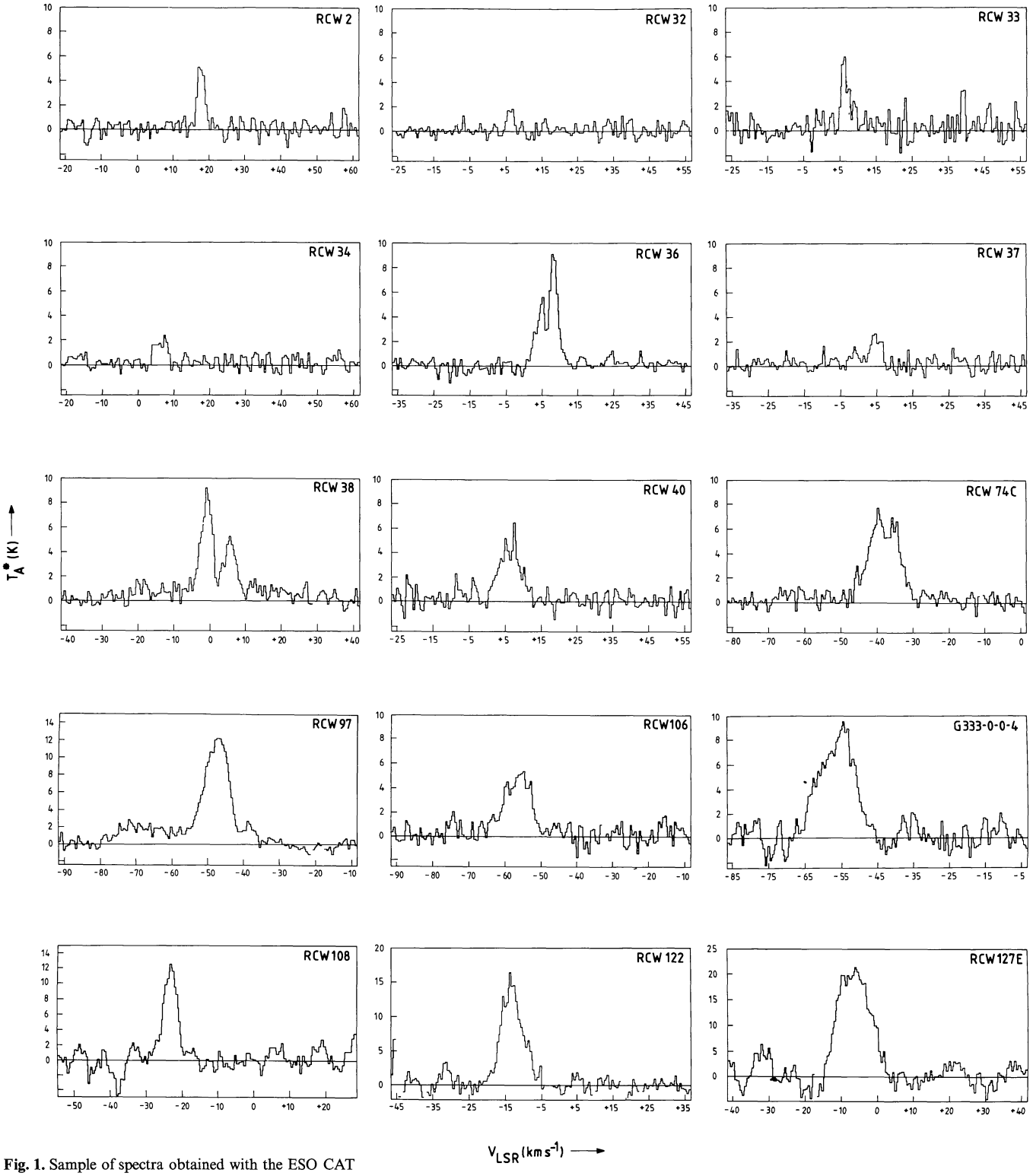


**Fig. 1.** Sample of spectra obtained with the ESO CAT

source like Orion-A beam dilution will lead to smaller antenna temperatures for observations with larger beams. Likewise, for narrow (unresolved) lines a lower velocity resolution may lead to a decrease in antenna temperature. A more serious obstacle to a realistic comparison of the various CO surveys is the calibration used to obtain the quoted "$T_A^*$"-values. Apart from atmospheric and telescope losses, measured temperatures should be corrected also for a beam coupling efficiency. This requires both knowledge about the brightness structure of the source and the beam profile. The former is usually not known and the latter, as in our case, only to some degree. This problem prompted Kutner and Ulich (1981) to suggest a more uniform way to report CO data, so that it is clear

**Table 2b.** Comparison CO data; $T_A^*$ (K)

| | (1) | (2) | (3) | (4) | mean | |
|---|---|---|---|---|---|---|
| Transition | 2→1 | 2→1 | 1→0 | 1→0 | 2→1 | 1→0 |
| HPBW | 5′.5 | 1′.6 | 2′.8 | 4′.5 | | |
| Source | | | | | | |
| Orion-A | 35.6 | 65 | 65 | 45 | 1.0 | 1.0 |
| RCW 36 | 9.4 | 11.9 | 14.1 | 11 | 0.22 | 0.23 |
| RCW 38 | 9.1 | 15.5 | 9.7 | 11.3 | 0.25 | 0.25 |
| RCW 42 | 2.8 | < 4.5 | 2.0: | 4.6 | 0.08: | 0.07: |
| RCW 57 | 9.9 | 27.5 | 18.1 | 29 | 0.35 | 0.46 |
| RCW 74B | 8.5[a] | < 2.5 | 12.0 | 9.1 | 0.24: | 0.19 |
| RCW 74C | 7.6 | 11.9 | 18.3 | 19.3 | 0.20 | 0.36 |
| RCW 92 | 7.7 | 17.9 | 27.0 | 20.2 | 0.25 | 0.43 |
| RCW 97 | 12.2 | 19.0 | 22.3 | 27.2 | 0.32 | 0.47 |
| RCW 106 | 5.2 | 4.4 | 11.7 | 11.8 | 0.11 | 0.22 |
| G333.0−0.4 | 9.5 | 14.7 | 24.3 | 25.0 | 0.25 | 0.46 |
| RCW 108 | 12.7 | 17.6 | 13.7 | 21.2 | 0.31 | 0.34 |
| RCW 122 | 16.6 | 17.6 | 34.8 | 33 | 0.37 | 0.63 |
| RCW 127D | 9.2[a] | 21.6 | 37.2 | 33 | 0.30 | 0.65 |
| RCW 127E | 20.8 | – | 34.5 | 37 | 0.58: | 0.68 |
| G351−1.3 | 13.7 | 16.6 | 24.0 | 34 | 0.32 | 0.56 |
| W22 | 7.8 | 7.1 | 10.7 | 15 | 0.16 | 0.25 |
| W22B | 5[a] | 8.1 | 13.6 | 21 | 0.13: | 0.34 |

*Notes to Table 2b*
(1) This work; velocity resolution = 0.33/1.3 km s$^{-1}$
(2) Martin et al. (1983); velocity resolution = 1.3 km s$^{-1}$
(3) Whiteoak et al. (1982); velocity resolution = 0.6 km s$^{-1}$
(4) Gillespie et al. (1977); velocity resolution = 2.6 km s$^{-1}$
[a] Poor quality spectrum

**Table 2c.** Ratios of antenna temperatures $T_A^*$

| Ratio | Remarks | |
|---|---|---|
| $T_A^*$ (this paper)/$T_A^*$ (M83) | 1.3±0.1 | same transition different beam widths |
| $T_A^*$(WOR82)/$T_A^*$(G77) | 0.63±0.04 | same transition different beam widths |
| $T_A^*$ (this paper)/$T_A^*$(G77) | 0.65±0.1 | different transitions same beam width |
| $T_A^*$(M83)/$T_A^*$(WOR82) | 0.9±0.1 | different transitions same beam width |
| $T_A^*$ (this paper)/$T_A^*$(WOR82) | 1.0±0.1 | different transitions different beam widths |
| $T_A^*$(M83)/$T_A^*$(G77) | 0.49±0.1 | different transitions different beam widths |
| $\langle T_A^*(2\rightarrow1)\rangle/\langle T_A^*(1\rightarrow0)\rangle$ | 0.73±0.1 | ratio of average |

which correction factors have been included. As it is, however, the measured antenna temperatures are either scaled to an assumed value of $T_A^*$ for Orion-A (e.g. $T_A^*$ = 65 K), or the reader is left in some doubt as to what corrections were actually applied. For this reason, a comparison of the numbers in Table 2b is only possible qualitatively. We have chosen to judge all other sources relative to Orion-A instead of trusting the absolute values of the temperatures given. Table 2c gives the average ratios of sources in Table 2b, when we first scale all temperatures of a particular survey to the Orion-A temperature as it is measured (or adopted) in that survey. Then, from the above and from Table 2c, we conclude that first of all there is a large scatter in the various ratios, from which one cannot infer any difference in temperature between the two transitions considered, other than that the G77 $T_A^*$-values are somewhat too high, with respect to the other data. At the same time, our data are somewhat too high (or the M83-data too low). Therefore, the CO in the sources detected is optically thick and thermalized.

Fewer uncertainties are involved when velocities are considered. Comparing the CO velocities in Table 2a with those measured for H109α, CS and $H_2CO$ (collected from Wilson et al., 1970; Gardner and Whiteoak, 1978; and WOR82) we find no systematic velocity difference between the ionized gas and the molecular cloud nor between the three species of molecules. However, for individual sources (such as Orion-A) velocity difference may be present. It should be noted that the comparison has been made at the positions where CO was observed; a different situation may be found when mapping around this position.

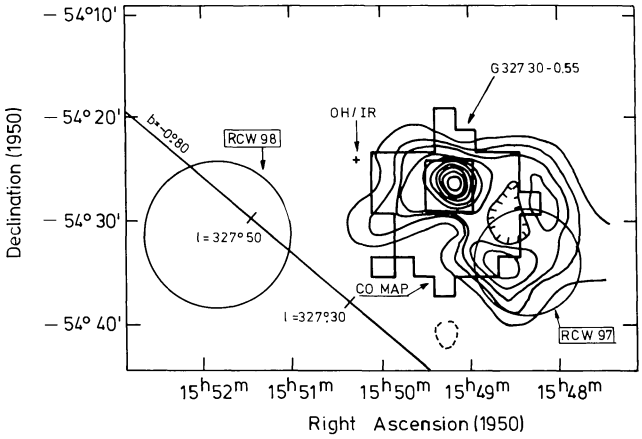


**Fig. 2.** 408 MHz continuum survey around G327.3−0.6 (taken from Goss and Shaver, 1970). The area mapped in CO is indicated as well as the positions and approximate extent of the optical HII regions RCW 97 and RCW 98. The smaller square inside the CO map is the region mapped at 1415 MHz by Retallack (1980)

## 4. Mapping results

### 4.1. G327.3−0.6

The optical HII region RCW 97 is associated with a minor peak in a complex of radio continuum sources. The major radio peak G327.3−0.6 is offset by about 10′ to the NE. The overall 408 MHz radio structure of the region (Goss and Shaver, 1970) is shown in Fig. 2. The circles in this radio map represent the approximate boundaries of RCW 97 and RCW 98, taken from photographs published by Georgelin and Georgelin (1970).

RCW 97 and RCW 98, together with RCW 96, RCW 99, a few other optical HII regions, and some HII regions of which only H109α line data are available (Wilson et al., 1970), all seem to be part of a single complex, centered at $l$ = 328°.0, $b$ = −0°.5 (also known as Norma I region), with a mean radial velocity

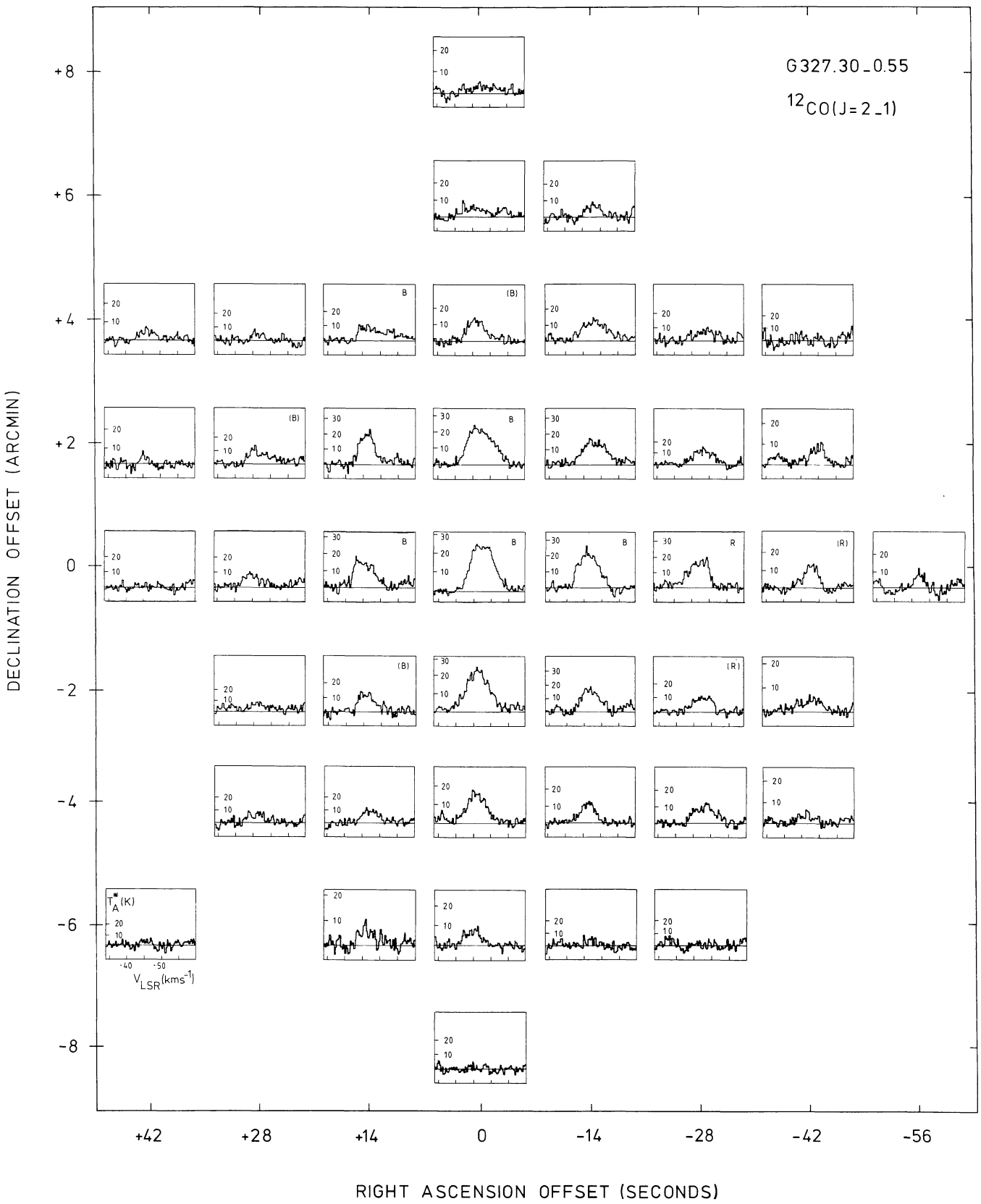


**Fig. 3.** The CO($J=2\rightarrow1$) spectra of G3273−0.6, obtained with the higher resolution (0.33 km s$^{-1}$) filterbank. Scales are indicated in the spectrum at ($+42^{s}, -6'$). RA and DEC offsets are with respect to $\alpha = 15^{h}49^{m}16^{s}$, $\delta = -54°28'24''$ (1950)

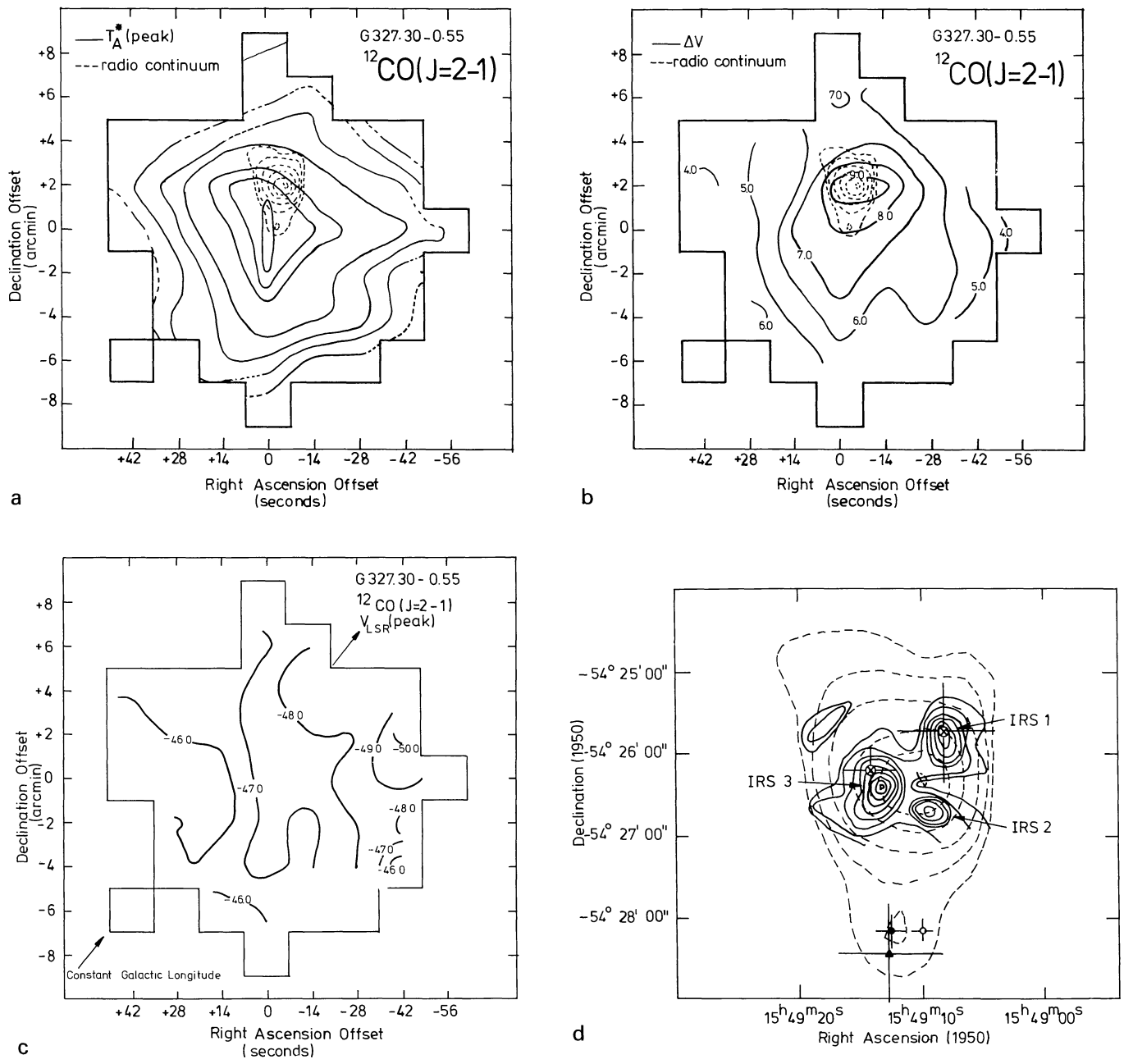


**Fig. 4a–d.** Summary of the CO($J=2\rightarrow1$) results for G3273−0.6. Offsets are all with respect to $\alpha=15^h49^m16^s$, $\delta=-54°28'24''$ (1950). Frames *a*, *b*, and *d* show the 1415 MHz contours (dashed; Retallack, 1980) for reference. **a** $T_A^*$ (peak) contours. Contour values 3, 6, 9, 12, 18, 21, and 23 K. **b** Linewidth, $\Delta V$; contours labeled in km s$^{-1}$. **c** Contours of constant velocity $V_{LSR}$. The numbers are in units of km s$^{-1}$. **d** The area around G3273−0.6, showing the 10 μm continuum contours (drawn; Frogel and Persson, 1974). Positions of OH 1665 MHz (▲) and 1612 MHz (⊗), $H_2O$ (●), and 3.6 μm (○) are also indicated

$V_{LSR}=-46$ km s$^{-1}$, corresponding to a (near) kinematic distance of 3.4 kpc (Georgelin and Georgelin, 1976).

We have made a first attempt at studying the complex by mapping CO associated with the strong radio peak G327.3−0.6 with the 2.5 m telescope at Las Campanas. This source was studied in detail by Retallack (1980) at 1415 MHz continuum. Several atomic and molecular species have already been observed in this direction; the presence of several high-excitation molecules [such as $NH_3$ (Batchelor et al., 1977), CS (Gardner and Whiteoak, 1978), HCN (Whiteoak and Gardner, 1978)] detected at the position of the stronger radio source, indicates molecular gas of high density ($n(H_2)\geqq10^4$ cm$^{-3}$). Star formation activity in this dense molecular cloud is indicated by the presence of several classical signposts such as infrared emission (see e.g. Persson et al., 1976; Epchtein and Lépine, 1981), OH/$H_2O$ maser emission (e.g. Caswell et al., 1980; Batchelor et al., 1980). The visual extinction $A_V$ towards the infrared sources is at least 20 magnitudes (e.g. Persson et al., 1976).

We mapped an area of about 14′ × 14′ around the radio peaks; the boundaries are indicated by solid lines in Fig. 2. The area is slightly undersampled by beams spaced 2′.5 apart. At the full spectral resolution of 0.33 km s$^{-1}$, the rms noise is about $T_A^*=1.5$ K. Individual spectra are shown in Fig. 3, and

maps of corrected antenna temperature, $T_A^*$, linewidth, $\Delta V\left[=\int_{\text{line}} T_A^* dV/T_A^*(\text{peak})\right]$, and $V_{\text{LSR}}$ (velocity of the peak of the line with respect to the Local Standard of Rest) in Fig. 4a–c. Offsets refer to a zero position with $\alpha(1950)=5^h49^m16^s$ and $\delta(1950)=-54°28'24''$. For comparison we have shown a map of the compact radio continuum source, 10 μm infrared sources and $OH/H_2O$ maser positions (Fig. 4d). The area shown in Fig. 4d corresponds to the rectangle in Fig. 2.

The radial velocity contours drawn in Fig. 4c are based on velocities at the line peak position, and have an uncertainty of 0.8 km s$^{-1}$. There is a progression of blue to red velocities from NW to SE in a direction that deviates 60° from the direction of constant galactic latitude. The total change in velocity is 3 to 4 km s$^{-1}$ over about 5′ (5 pc); the points in the SW part of the map do not constitute a significant deviation from this general trend as the S/N-ratio of the spectra is quite low. It is not clear whether this gradient extends to the very east of the map or to somewhere near the line $\Delta\alpha=+10^s$, because the whole region between $\Delta\alpha=+42^s$ and $\Delta\alpha=+10^s$ seems to be at a constant velocity of $-46$ km s$^{-1}$.

The velocity shift could be interpreted as being due to rotation; however, $^{12}CO$ (optically thick) observations are not indicative for the bulk of the gas, so observations of density-sensitive molecules would be necessary to confirm this.

Figure 4d shows the major sites for star formation. The main radio peak shows considerable structure in the infrared, and subtends an area about 2′ across (about 2 pc at the distance of 3.4 kpc). The lesser site is displaced to the south by about 2′ (2 pc, assuming it is at the same distance as the main radio peak) and has a size of about 0.′5 (0.5 pc). It appears to be less evolved, and is therefore most likely younger. It is this presumably most recent site of star formation that very nearly coincides with the CO peak $T_A^*=23$ K. The northern site, on the other hand, coincides very closely with the position of peak velocity width $\Delta V=9.5$ km s$^{-1}$, in accordance with what one would expect for a more evolved site of interaction between a newly formed star and its surroundings.

The molecular cloud associated with these star formation sites has a size, as defined by the $2\sigma$ ($T_A^*=3$ K) contour, of $11'\times 15'$ ($11\times 15$ pc$^2$), with an extension to the west, in the direction of a weak, extended 408 MHz continuum source (see Fig. 2). There is no extension in the antenna temperature distribution towards RCW 97 and its associated continuum source.

In addition to CO($J=2\rightarrow 1$) we have also observed HCN($3\rightarrow 2$) emission ($\nu=265.886$ GHz) at the central position, and at positions displaced 90″ to the east and west. This HCN emission, implying densities $n(H_2)\geqq 10^4$ cm$^{-3}$, peaks sharply at the central position, indicating that the southern star formation site is found at a position of relative maximum density of the cloud.

Retallack (1980) gives a flux density $S(1.4\,\text{GHz})=23$ Jy for the whole complex; we estimate about 1 Jy to be due to the southern extension. At a distance of 3.4 kpc this then yields excitation parameters $u=86$ pc cm$^{-2}$ and $u=30$ pc cm$^{-2}$ for the two sites. (For an HII region, the parameter $u$ is a measure of the number of ionizing photons emitted by the exciting star and is therefore related to the stellar spectral type; at a frequency $\nu=1.4$ GHz and electron temperature $T_e=10^4$ K, $u/\text{pc cm}^{-2}=13.5\,(S/\text{Jy})^{1/3}(D/\text{kpc})^{2/3}$.) This in turn corresponds to excitation by respectively an O9.5 and an O5.5 star, or the ionizing equivalent (Panagia, 1973). We note that the projected linear distance of 2 pc between the two star formation sites, a space density of $n(H_2)\geqq 10^4$ cm$^{-3}$ and the relative stage of evolution are consistent with the Elmegreen and Lada (1977) sequential star formation model: substituting the parameters of the two source components in their Eqs. (19a) and (19b) we obtain a typical separation of 2.4 pc and a typical age difference of $8\,10^5$ years, corresponding to a mean velocity of about 1 km s$^{-1}$ for the movement of the northern ionization fronts into the molecular cloud.

Another interesting aspect of the G327.3−0.6 cloud can be seen in Fig. 3: several of the CO profiles are clearly asymmetric. In order to bring out the asymmetries and determine the CO distribution in the shoulders, we integrated over the line shoulders at each measured position (line shoulders are defined here as those parts of the line profile for which $T_A^*>T_{\text{rms}}$ and $V_{\text{LSR}}>V(T_{\text{peak}})+\frac{1}{2}\Delta V$ and $V_{\text{LSR}}<V(T_{\text{peak}})-\frac{1}{2}\Delta V$). Maps of the red and blue shoulders thus defined are shown in Fig. 5.

A clear separation is seen between positions where blue wings dominate (N and NE) and those where the red wings are more pronounced (S and W). Both the blue and red wings have in fact two positions at which they peak; the separation between the peaks is 4′ (4 pc) in both cases. The centres of the lines connecting respectively the blue and red peaks are at a projected distance of 5.′3 (=5 pc). Projecting Fig. 4d onto 5a and b, we find that the position of the southern and youngest star formation site (indicated by the cross in Fig. 5a and b) is at the centres of the lines connecting the blue and red peaks.

Spherically symmetrical collapse or expansion as the cause of the asymmetrically broadened CO lines is ruled out by the anisotropic spatial distribution of the blue and red intensities. A possible explanation for the CO observations is a bipolar gas outflow. This phenomenon has by now been detected in several sources and the pattern as it is seen in G327.3−0.6 is very similar to that in the confirmed cases (Bally and Lada, 1983). Asymmetric profiles do not, however, a priori imply outflow. If for instance the shoulders or wings of the profile are more optically thin than the centre of the line we look deeper into the cloud and may be seeing coherent internal motions of individual parcels of gas in the cloud (rotation), which are not visible in the centre of the line where we only see the outermost layer of the cloud. The only way to determine whether we are seeing outflow is to establish whether the cloud's mass is large enough to gravitationally bind the material seen in the shoulders or wings of the line. As an (admittedly crude) rule of thumb, we use $N_{\text{H}}=I_{12}\,1.0\,(\pm 0.5)\,10^{21}$ cm$^{-2}$, with $I_{12}=\int_{\text{line}} T_A^* dV$ in K km s$^{-1}$ (Liszt, 1982). For the gas corresponding to that part of the line profile that is contained within $\Delta V$ around the line velocity (i.e., the bulk of the cloud, not the shoulders or wings) we find that $I_{12}=50$ K km s$^{-1}$, using all positions within the observed area where signal was detected. This implies a lower limit ($\tau\gg 1$) to the mass of 6.3 $(\pm 3.2)\,10^4 M_\odot$ and thus a lower limit to the escape velocity, $v_e$, of $9.1\,(^{+2.0}_{-2.7})$ km s$^{-1}$. The projected velocity excess of the CO in the line shoulders is of the order of 3.5 km s$^{-1}$ on average, which is less than $v_e$ and would thus argue against an outflow scenario. On the other hand, the evidence is not clear-cut. First of all, $^{12}CO$ is not a density-sensitive molecule and any derivation of mass from observations of $^{12}CO$ is very uncertain. Secondly, the spectra are noisy ($T_{\text{rms}}=1.5$ K) which results in uncertain values for the integral $I_{12}$ and prevents detection of low intensity wings, while the sources identified with outflow have high-velocity wings at the $T_A^*=0.1$ K level or lower (Bally and Lada, 1983). This, together with the suggestive apparance of the cloud in CO (Fig. 5a and b) and the fact that the excess velocity we do detect is a lower limit due to projection effects, make G327.3−0.6 a candidate for a bipolar outflow source and certainly worthy of further observations.

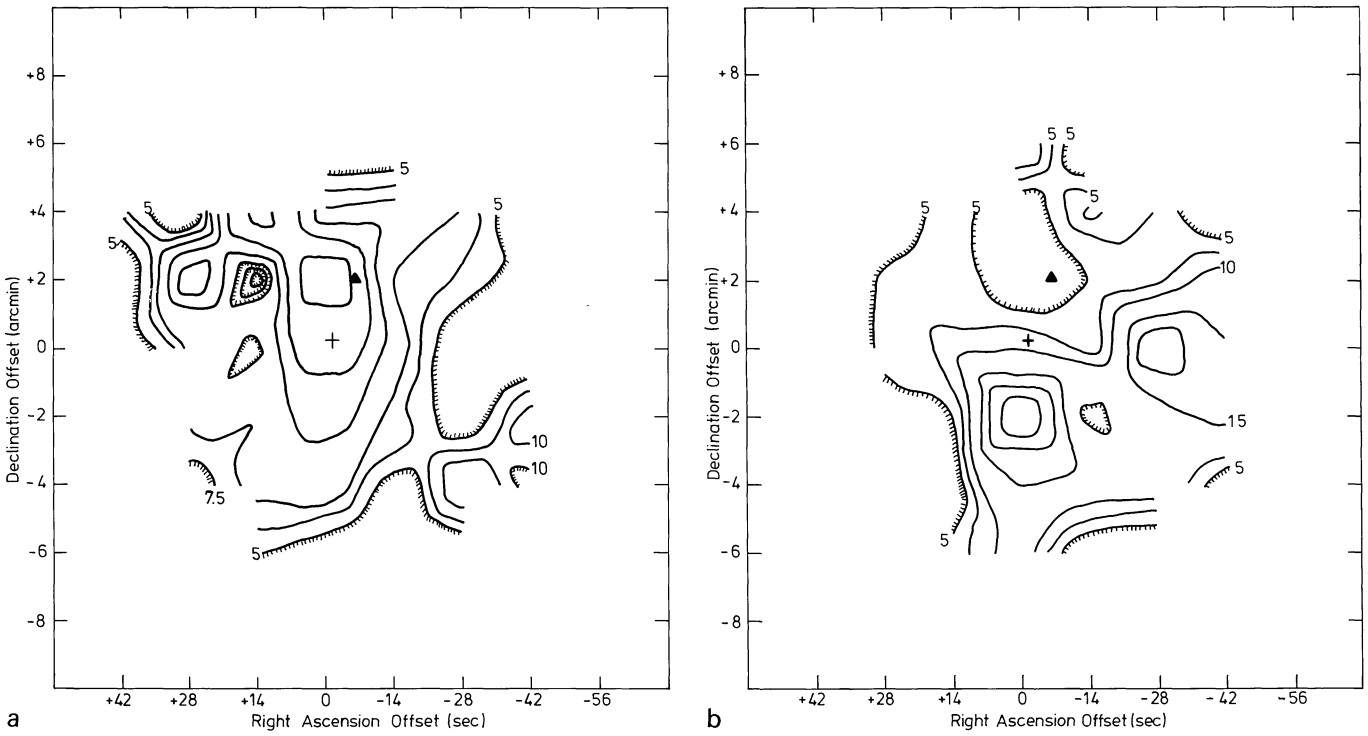


**Fig. 5a and b.** Contours of $\int T_A^* dV$ *for G327.3−0.6.* Integration is performed over those parts of the line profile for which $T_A^* > T_{rms}$, and $V_{LSR} > V(T^*_{peak}) + \frac{1}{2}\Delta V$ (red shoulder) and $V_{LSR} < V(T^*_{peak}) - \frac{1}{2}\Delta V$ (blue shoulder). Contour values are 5. 7.5, 10, 15, 20, and 30 K km s$^{-1}$. For reference we show the main radio peak/IR sources (▲) and the secondary radio peak/OH, $H_2O$ maser/3.6 μm emission (+). **a** Blue shoulder. **b** Red shoulder

If what we see in CO is indeed the signature of outflow, we can estimate some parameters of the flow, following Rodriguez et al. (1982). With a mean separation $r$ between the lobes and the "exciting" source of about 3 pc and a CO velocity spread $V$ of about 9.5 km s$^{-1}$, the dynamical timescale $r/V$ is about $3\,10^5$ yr, which is similar to the timescales found for other bipolar outflow sources, and also in good agreement with the small age expected from the sequential star formation model (see above).

Rough lower limits to the mass and mechanical energy of the flow can be obtained by assuming that the CO in the wings is optically thin. For this case, Rodriguez et al. (1982) calculate the mass in $H_2$ molecules from $v$ to $v+dv$; $v$ is the radial velocity with respect to the line centre. Using their equation and substituting typical values for this source [$T_A^* = 5$ K (in the shoulders), $T_{exc} = 15$ K, $dv = 4$ km s$^{-1}$, distance $D = 3.4$ kpc, major and minor diameter of the emitting zone resp. $\theta_a = 2'$ and $\theta_b = 1'$], we find for the mass in $H_2$ molecules contained in the flow $dM(H_2) \geqq 4 M_\odot$ per lobe. This corresponds to a mechanical energy $\frac{1}{2}Mv^2$ of at least $0.5\,10^{45}$ erg. These values, again, are similar to some of those quoted by Rodriguez et al. (1982).

We summarize our results on G327.3−0.6 as follows. The strongest radio peak in this complex containing the visible HII region RCW 97 is associated with a fairly compact (typical size ~ 13 pc) and locally dense ($n(H_2) \geqq 10^4$ cm$^{-3}$) CO cloud. The radio source consists of a relatively evolved HII region (complex) of age $\sim 10^6$ years offset by about 2 pc from the centre of the cloud. At the centre, under circumstances indicating sequential star formation in agreement with the Elmegreen and Lada model, a much less evolved compact HII region is found, accompanied by OH/$H_2O$ maser emission. This compact HII region appears to be a centre of bipolar outflow, with a characteristic age of about $10^5$ years.

### *4.2. G35.2−1.8*

The HII region complex G35.2−1.8 (W48) lies about 1°3 to the east of the supernova remnant W44, which corresponds to a projected distance of 75 pc, since both sources lie at the same distance of 3.4 kpc (Clark and Caswell, 1976). The Palomar Sky Survey prints of this region show the presence of strong extinction (caused largely by the dark cloud Khavtassi 3 (Khavtassi, 1960)), and there is no indication of an optical counterpart to W48.

Radio continuum observations show that W48 is a triple source, with a strong central component, G35.2−1.8 (hereafter called W48A), and two weak, extended components, G35.1−1.5 and G35.4−1.8 (hereafter called W48B and W48C, respectively).

Most studies of W48 concentrate on the strong central component W48A. Interferometric radio continuum observations of this component reveal that it actually consists of several compact components. Evans et al. (1979) found two ultra-compact sources (1″.8 and <8″), and one compact source (30″ × 60″) at 3.5 μm. For a distance of 3.4 kpc the sizes of these sources are 0.03 pc, 0.13 pc and 0.5 × 1.0 pc$^2$, respectively, W48 has been observed in several atomic and molecular species. The infrared source AFGL 2304 coincides with W48. Several authors have published near-infrared source positions (Dyck and Simon, 1977; Zeilik and Lada, 1978; Evans et al., 1979) but there seems to be little agreement between them. From the 3.5 μm map published by Zeilik and Lada (1978) we infer that at least W48A is a region of active star formation.

Pashchenko (1977) was the first to raise the possibility that W48 and W44 are related. The CO observations by Dame (1983, and references therein), in combination with the OH absorption observations of Goss et al. (1971) of this region suggest that both sources are situated in one giant molecular cloud with an

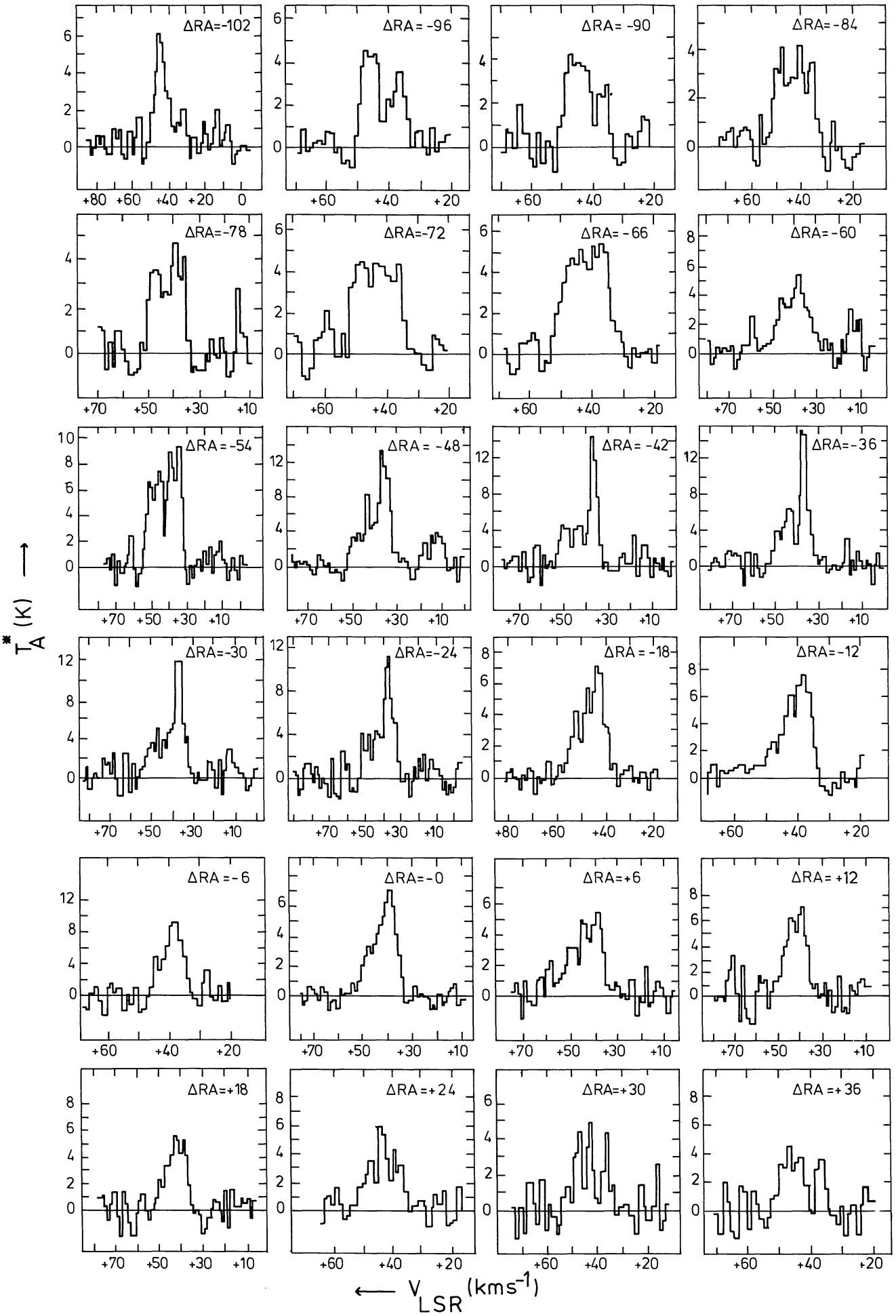


**Fig. 6.** The CO($J=2\rightarrow1$) spectra for W48 obtained with the lower resolution (1.3 km s$^{-1}$) filterbank. Offsets are in s with respect to $\alpha=18^h59^m15^s$ (1950), while $\delta=+01°08'00''$ (1950) for all observed positions

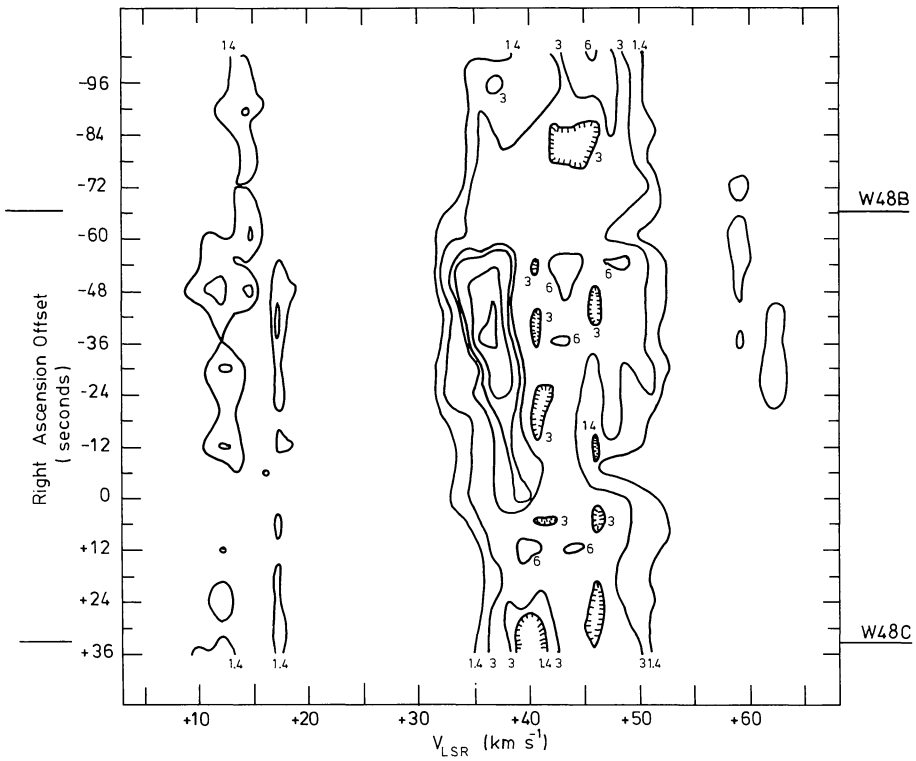


**Fig. 7.** Position vs. velocity map of the strip scan through W48 at $\delta = +01°08'00''$ (1950). Contour values are $T_A^* = 1.4$, 3, 6, 7, 10, and 14 K. The zero position is at $\alpha = 18^h59^m15^s$ (1950). Velocity resolution is 1.3 km s$^{-1}$

approximate size of $120 \times 60$ pc$^2$. Dame (1983) infers from his observations that nearly all emission between $l = 34°$ and $l = 36°$, with velocities ($V_{LSR}$) between $+30$ km s$^{-1}$ and $+50$ km s$^{-1}$, and probably much of the emission at the same longitudes between $+50$ km s$^{-1}$ and $+65$ km s$^{-1}$, is associated with W44.

An area of about $20' \times 20'$ around W48A has been mapped in CO($J = 1 \rightarrow 0$) by Zeilik and Lada (1978). They found two concentrations separated by about 6′, one of which is close to, but not coincident with, the compact radio sources constituting W48A (2′ west). Other CO observations made by Wilson et al. (1974) and Scoville and Wannier (1979) among other things show peaks near W48A.

Using the ESO 3.6 m telescope, we fully sampled a 35′ long strip through W48 (at constant $\delta(1950) = +01°08'$) with a beam separation of 1.′5 in the CO($J = 2 \rightarrow 1$) transition. The individual profiles are shown in Fig. 6, and the resulting map is shown in Fig. 7.

Right ascension offsets are given with respect to the centre of W48A ($\alpha(1950) = 18^h59^m15^s$). One sigma rms noise is 1.4 K at a velocity resolution of 1.3 km s$^{-1}$. We make no use of the higher-velocity resolution data because the noise is quite high, and the lines are broad.

Two major features are seen: a narrow one at $V_{LSR} = +14.5$ km s$^{-1}$, with $\Delta V = 2$ km s$^{-1}$, and a much broader one between $V_{LSR} = +35$ km s$^{-1}$ and $+50$ km s$^{-1}$, that is associated with the W48 complex. Between $\Delta\alpha = -90^s$ and $\Delta\alpha = -60^s$, line profiles of this broad component are flat topped; between $\Delta\alpha = -48^s$ and $\Delta\alpha = +6^s$ they show a pronounced asymmetry over most of this range in the form of a narrow spike at the low-velocity side, with a broad wing at the high-velocity side. The spike has a velocity of about $+37$ km s$^{-1}$. It would be tempting to ascribe this line shape to the effects of self absorption, in particular because the pronounced asymmetry coincides with maximum line width at low intensity levels, and because the spike is shifted from the mean velocity of more symmetrical profiles (cf. Figs. 6 and 7). On the other hand, blending of profiles due to two different clouds cannot be ruled out, particularly in view of the presence of two $H_2CO$ absorption dips at $V_{LSR} = +37$ km s$^{-1}$ and $V_{LSR} = +44$ km s$^{-1}$ (the second being the strongest) seen with a comparable beam size (Downes et al., 1980). Thus the matter is as yet inconclusive.

The CO cloud (mean size 5′ or 5 pc) mapped by Zeilik and Lada (1978) corresponds to part of the "spike" at $V_{LSR} = +37$ km s$^{-1}$ between $\Delta\alpha = -10^s$ and $\Delta\alpha = 0^s$. From Fig. 7 it is clear that this cloud is part of a larger CO complex, stretching from about $\Delta\alpha = -80^s$ to $\Delta\alpha = +18^s$, i.e. over a length of about 25 pc. As already noticed by Zeilik and Lada (1978), the velocity difference between the CO cloud complex and the HII regions together with the lack of an optical counterpart to the radio regions are consistent with W48A, B and C being blisters (Israel, 1978) on the far side of the cloud.

The narrow feature has a peak velocity of $V_{LSR} = +14.5$ km s$^{-1}$ and a width $\Delta V = 2$ km s$^{-1}$ between $\Delta\alpha = -54^s$ and $\Delta\alpha = -102^s$, and splits symmetrically into two lines at $\Delta\alpha \simeq -48^s$. The radial velocity of these two lines is $+12$ km s$^{-1}$ and $+17.2$ km s$^{-1}$, with widths respectively $\Delta V \simeq 2$ km s$^{-1}$ and 1 km s$^{-1}$. The splitting occurs over a range of at least 21′. This narrow feature is apparently associated with the foreground cloud Khavtassi 3 (see also Wooten, 1977). The line splitting can be interpreted by the line of sight passing through various other clouds as the Right Ascension increases.

### 4.3. *G265.1+1.5*

G 265.1+1.5 (RCW 36) is an optical HII region, situated in a dust lane extending several degrees along a line of constant right ascension, as can be seen on Palomar Observatory Sky Survey (POSS) prints. This dust lane cuts through several HII regions and lies at the north-eastern edge of the Gum nebula. From $H_2CO$ and

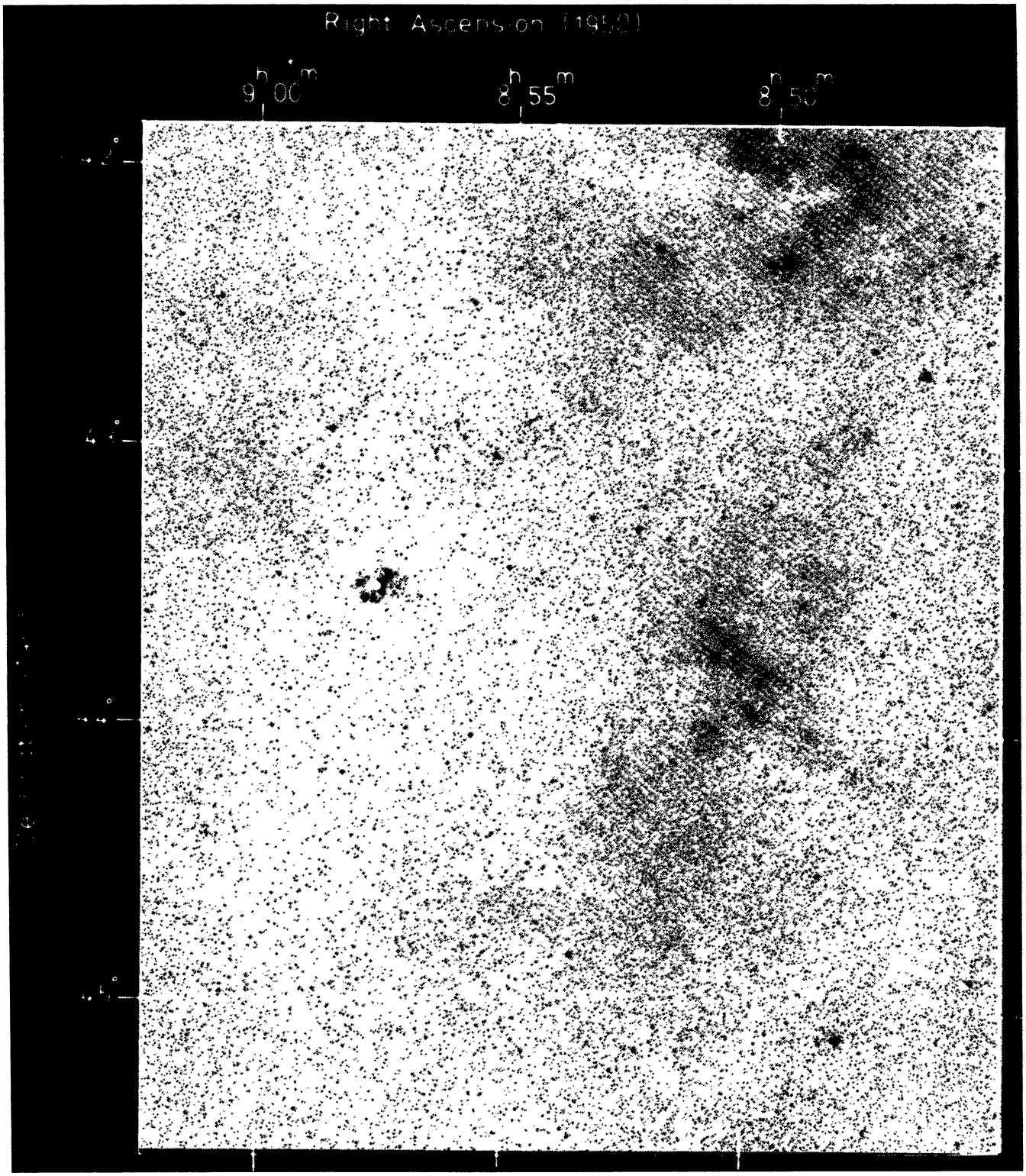


**Fig. 8a.** The area around the optical HII region RCW 36, reproduced from a POSS-E print. Observed positions are indicated

OH observations, Whiteoak and Gardner (1977) conclude that this dust lane is associated with a dense elongated molecular cloud.

With the CAT, we have obtained spectra at 23 positions in the dust cloud. The observed positions are shown on a copy of the POSS print of the region in Fig. 8a; the spectra are collected in Fig. 8b. The spectrum taken at the central position is shown in Fig. 1.

With a detection limit of $T_A^* = 1$ K, we find CO at 20 of these positions. The three northernmost detections were obtained in the dust lane cutting across the optical HII region RCW 33. At these

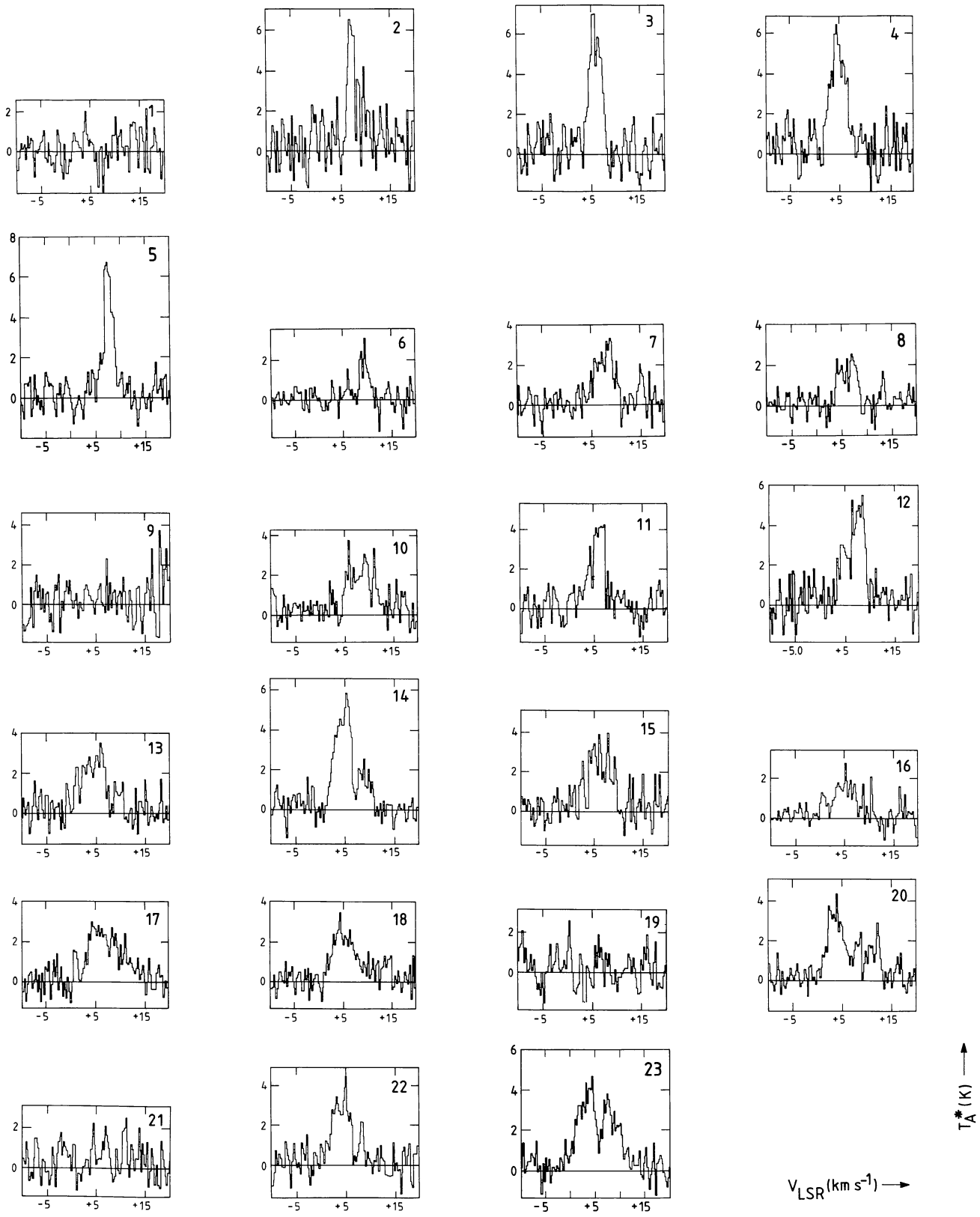


**Fig. 8b.** CO($J=2\rightarrow1$) spectra taken in the dust cloud against which RCW 36 is seen projected; numbers on the spectra correspond with the numbered positions in Fig. 8a

positions, emission is quite strong with $T_A^* = 6$ K to 7 K; going from east to west in this dust lane the line velocity increases from $V_{LSR} = +4.4\,km\,s^{-1}$ to $V_{LSR} = +7.2\,km\,s^{-1}$ over a distance of 19′.4. All other detections were made in the dust cloud stretching roughly north-south, which has RCW 36 projected on (or embedded in) it. [Positions 5 and 8 coincidence with the nebulae vBH27b (reflection nebula) and vBH 25a (a.k.a. RCW 34), respectively.] The spectra reveal that there are two components present in that cloud; their velocities are +3 to $+5.5\,km\,s^{-1}$ and +7 to $+9\,km\,s^{-1}$. Both of them peak at the position of RCW 36. The higher-velocity component can be traced over the whole area observed, except at three positions, where the line velocity is intermediate at $V_{LSR} = +5.9\,km\,s^{-1}$ (Position 15), $V_{LSR} = 6.3\,km\,s^{-1}$ (Position 2), and $6.6\,km\,s^{-1}$ (Position 11). The two spectra obtained 0°.5 south of RCW 36 (Position 17 and 18) are probably a blend of the two components: the line peak is at the lower velocity, but the lines are broad ($\Delta V = 5.5\,km\,s^{-1}$ and $\Delta V = 7.4\,km\,s^{-1}$) and asymmetric, being steeper to the low-velocity side.

The lower-velocity component is only found at positions south of RCW 36. One of the spectra in that part of the cloud (at Position 20) shows an additional line at $V_{LSR} = +12\,km\,s^{-1}$. (There are indications of a higher velocity component at Positions 7 and 8 as well, though less clear than at Position 20.) There is no obvious systematic trend in the velocities over the dust cloud. The widths of the two emission components are comparable ($\Delta V \simeq 3.2\,km\,s^{-1}$). Thus, from the CO data we conclude that we are seeing at least two, and at one point possibly three clouds or cloud components in the line of sight. The velocities of these clouds range from about $+3.3\,km\,s^{-1}$ to $+9.2\,km\,s^{-1}$ (at one point up to +12 or $+15\,km\,s^{-1}$), with values of $T_A^*$ between the noise level of 1 K up to 9.4 K.

These observations agree well with those of $H_2CO$ by Whiteoak and Gardner (1977), who mapped an area of the dustlane containing 17 of our data points. They find absorption at velocities between $+3\,km\,s^{-1}$ and $+9\,km\,s^{-1}$. Their map of $H_2CO$ absorption shows the lower-velocity component to be most prominent south of RCW 36, whereas the higher-velocity component dominates north of RCW 36. Around the optical H II region, $H_2CO$ is seen in absorption over the whole range of velocities shown ($+3.8\,km\,s^{-1}$ to $+8.7\,km\,s^{-1}$), consistent with our finding of two velocity components in CO in spectra taken close to RCW 36.

The ratio $R$ of the minimum $H_2CO$ temperature and the maximum CO temperature as a function of $T_A^*$(CO) shows a trend in the sense that at positions south of RCW 36 the ratio is higher than at points north of the H II region. We take this as an indication that we see a predominance of denser clumps of material in the southern part of the observed cloud as compared with further to the north.

## 4. Summary

The data presented and discussed in the previous sections can be summarized as follows:

(i) we have looked for CO($J = 2 \rightarrow 1$) emission at single positions near 47 (mostly southern) H II regions. Twenty eight of these yielded detections. It seems that on average, and within the measurement errors, the strengths of the $J = 2 \rightarrow 1$ and the $J = 1 \rightarrow 0$ ransitions of CO are equal for those regions in our sample that have also been included in other surveys. A detailed comparison is hampered by uncertainties of the calibration and differences in beam size (and velocity resolution) used by the various observers.

(ii) the molecular cloud associated with G327.3−0.6 is an active site of star formation; the CO map shows a clear distinction between red and blue shifted emission, the two emission lobes being placed symmetrically around the secondary radio peak, which appears to be the youngest star formation site. The data are consistent with the source being of the type that has bipolar outflow. Rough estimates give a total mass of the $H_2$ molecules in the suspected flow of $\geqq 8 M_\odot$ and a total mechanical energy of some $10^{45}$ erg.

(iii) the CO line profiles in the direction of W48 are complex and could reflect either self absorption or blending. The observations are consistent with W48A, B, and C being blisters on the far side of the cloud.

(iv) the obscuration against which RCW 36 is seen in projection consists of clouds or cloud components at two or three separate velocities. The CO distribution agrees very well with that of $H_2CO$.

*Acknowledgements.* We thank the technical staffs at ESO La Silla and at Las Campanas Observatory for their support during our observing runs. We are grateful to Dr. Woltjer for allowing us a generous amount of time at the CAT for our experiments. Drs. Fitton and Page of ESA are thanked for their support and interest. We are much indebted to Dr. Sverre Lidholm from the University of Cork, Ireland, for his work on the receiver at La Silla. We highly appreciate Messrs. J. van der Biezen, J. van Amerongen, and I. Nagtegaal for their technical support and assistance with the observations, F. Cornelis for his software support and F. Selman from el Universidad de Chile for helping with the observations. Finally we thank Dr. John Bally for a valuable comment concerning G327.3−0.6.

## References

Batchelor, R.A., Gardner, F.F., Knowles, S.H., Mebold, U.: 1977, *Proc. Astron. Soc. Australia* **3**, 152
Batchelor, R.A., Caswell, J.L., Goss, W.M., Haynes, R.F., Knowles, S.H., Wellington, K.J.: 1980, *Austral. J. Phys.* **33**, 139
Bally, J., Lada, C.J.: 1983, *Astrophys. J.* **265**, 824
Blair, G.N., Peters, W.L., VandenBout, P.A.: 1975, *Astrophys. J. Letters* **200**, L161
Blitz, L., Fich, M., Stark, A.A.: 1982, *Astrophys. J. Suppl.* **49**, 183
Brand, J.: 1982, *ESO Messenger* **29**, 20
Brand, J.: 1983, in *Surveys of the Southern Galaxy*, eds. W.B. Burton, F.P. Israel, Reidel, Dordrecht, p. 223
Caswell, J.L., Haynes, R.F., Goss, W.M.: 1980, *Austral. J. Phys.* **33**, 639
Clark, D.H., Caswell, J.L.: 1976, *Monthly Notices Roy. Astron. Soc.* **174**, 267
Dame, T.M.: 1983, Ph. D. Thesis, Columbia Univ. N.Y.C.
De Graauw, Th., Lidholm, S., Fitton, B., Beckman, J., Israel, F.P., Nieuwenhuizen, H., Vermue, J.: 1980, *Astron. Astrophys.* **102**, 257
De Graauw, Th., Israel, F.P., De Vries, C.P.: 1983, in *Surveys of the Southern Galaxy*, eds. W.B. Burton, F.P. Israel, Reidel, Dordrecht, p. 17
De Vries, C.P., Brand, J., Israel, F.P., De Graauw, Th., Wouterloot, J.G.A., Van de Stadt, H., Habing, H.J.H.: 1984, *Astron. Astrophys.* Suppl. **56**, 333

Downes, D., Wilson, T.L., Bieging, J., Wink, J.: 1980, *Astron. Astrophys. Suppl.* **40**, 379
Dyck, H.M., Simon, T.: 1977, *Astron. J.* **211**, 421
Elmegreen, B.G., Lada, C.J.: 1977, *Astrophys. J.* **214**, 725
Epchtein, N., Lépine, J.R.D.: 1981, *Astron. Astrophys.* **99**, 210
Evans II, N.J., Beckwith, S., Brown, R.L., Gilmore, W.: 1979, *Astron. J.* **227**, 450
Frogel, J.A., Persson, S.E.: 1974, *Astrophys. J.* **192**, 351
Gardner, F.F., Whiteoak, J.B.: 1978, *Monthly Notices Roy. Astron. Soc.* **183**, 711
Georgelin, Y.P., Georgelin, Y.M.: 1970, *Astron. Astrophys. Suppl.* **3**, 1
Georgelin, Y.P., Georgelin, Y.M.: 1976, *Astron. Astrophys.* **49**, 57
Gillespie, A.R., Huggins, P.J., Sollner, T.C.L.G., Phillips, T.G., Gardner, F.F., Knowles, S.H.: 1977, *Astron. Astrophys.* **60**, 221
Gillespie, A.R., White, G.J., Watt, G.D.: 1977, *Monthly Notices Roy. Astron. Soc.* **186**, 383
Goss, W.M., Shaver, P.A.: 1970, *Austral. J. Phys. Astrophys. Suppl.* **14**, 1
Goss, W.M., Caswell, J.L., Robinson, B.J.: 1971, *Astron. Astrophys.* **14**, 481
Israel, F.P.: 1978, *Astron. Astrophys.* **70**, 769
Israel, F.P., de Graauw, Th., de Vries, C.P., Brand, J., van de Stadt, H., Habing, H.J.H., Wouterloot, J.G.A., van Amerongen, J., van der Biezen, J., Leene, A., Nagtegaal, I., Selman, F.: 1984, *Astron. Astrophys.* **134**, 396
Khavtassi, J., Sh.: 1960, Atlas of Galactic Dark Nebulae
Kutner, M.L., Ulich, B.L.: 1981, *Astrophys. J.* **250**, 341
Lidholm, S., De Graauw, Th.: 1979, Fourth International Conference on Infrared and Millimeter Waves and their Applications, Florida, ed. S. Perkowitz, p. App. 38
Liszt, H.S.: 1982, *Astrophys. J.* **262**, 198
Martin, R.N., Emerson, D.T., Ruf, K., Wilson, T.L., Zimmermann, P.: 1983, in *Surveys of the Southern Galaxy*, eds. W.B. Burton, F.P. Israel, Reidel, Dordrecht, p. 217
Panagia, N: 1973, *Astron. J.* **78**, 929
Pashchenko, M.I.: 1977, *Soviet Astron.* **21**, No. 2
Persson, S.E., Frogel, J.A., Aaronson, M.: 1976, *Astrophys. J.* **208**, 753
Retallack, D.S.: 1980, Ph. D. Thesis, Univ. of Sydney
Rodgers, A.W., Campbell, C.T., Whiteoak, J.B.: 1960, *Monthly Notices Roy. Astron. Soc.* **121**, 103
Rodriguez, L.F., Carral, P., Ho, P.T.P., Moran, J.M.: 1982, *Astrophys. J.* **260**, 635
Scoville, N.Z., Wannier, P.G.: 1979, *Astron. Astrophys.* **76**, 140
Ulich, B.L., Haas, R.W.: 1976, *Astrophys. J. Suppl.* **30**, 247
Whiteoak, J.B., Gardner, F.F.: 1977, *Proc. Astron. Soc. Australia* **3**, 147
Whiteoak, J.B., Gardner, F.F.: 1978, *Monthly Notices Roy. Astron. Soc.* **185**, 33p
Whiteoak, J.B., Otrupcek, R.E., Rennie, C.J.: 1982, *Proc. Astron. Soc. Australia* **4**, 434
Wilson, T.L., Mezger, P.G., Gardner, F.F., Milne, D.K.: 1970, *Astron. Astrophys.* **6**, 364
Wootten, H.A.: 1977, *Astrophys. J.* **216**, 440
Zeilik II, M., Lada, C.J.: 1978, *Astrophys. J.* **222**, 896